Organic Electronics 13 (2012) 1114–1120

Contents lists available at SciVerse ScienceDirect

Organic Electronics

journal homepage: www.elsevier.com/locate/orgel

Organic pin-diodes approaching ultra-high-frequencies

H. Kleemann [a,*], S. Schumann [b], U. Jörges [b], F. Ellinger [b], K. Leo [a], B. Lüssem [a]

[a] Institut für Angewandte Photophysik, Technische Universität Dresden, 01069 Dresden, Germany
[b] Lehrstuhl für Netzwerktheorie und Schaltungstechnik, Technische Universität Dresden, 01062 Dresden, Germany

ARTICLE INFO

Article history:
Received 8 February 2012
Received in revised form 7 March 2012
Accepted 7 March 2012
Available online 26 March 2012

Keywords:
Organic pin-diodes
Ultra-high-frequency diodes
Molecular doping
Organic rectifier circuits

ABSTRACT

Organic pin-diodes employing molecular doped hole and electron transport layers working at ultra-high-frequencies (UHF) are presented. In comparison to undoped organic Schottky diodes reported for ultra-high-frequency applications, the pin-concept is superior since the doping concentration and the intrinsic interlayer thickness can be adjusted in order to control the performance of such pin-diodes. We investigate the influence of both parameters on basic diode parameters like forward resistance and rectification ratio. In particular, we discuss the role of molecular doping and its influence on the AC signal response and we present an optimized doping ratio in order to accomplish highest charge carrier mobility and conductivity. Optimized devices are working as rectifiers up to 300 MHz at a small operating voltage of 2 V. The frequency limit is estimated to be at 1 GHz.

1. Introduction

Besides organic light-emitting diodes (OLED) and solar cells, organic diodes for UHF electronics have received a considerable attention. Namely, such UHF diodes are employed for high speed rectifiers in e.g. passive radio-frequency identification tags (RFID) [1–8]. RFID tags comprising organic diodes working at 13.56 MHz have been realized [6]. However, for certain applications, especially for high data transfer rate RFID tags, it is required to increase the cut-off frequency and to reduce the turn-on voltage (voltage where rectification starts) of the diodes simultaneously. This is challenging since the diode cut-off frequency behaves oppositely to the applied voltage across the diode. Im et al. [8] successfully used C_{60} Schottky diodes to overcome this problem and reported diodes approaching the GHz regime at low driving voltages of 2 V. This has been accomplished since in comparison to pentacene Schottky diodes [1,6], C_{60} has a higher charge carrier mobility and it forms low resistance contacts at one side and almost ideal Schottky barriers at the other contact. However, the ability of the Schottky diode concept is restricted to specific material combinations which is a significant technological limitation for device integration. To realize UHF electronic circuits based on organic semiconductors only a couple of materials and device concepts is suitable if limitations concerning processing and integrability are considered. The buckyball molecule C_{60} and pentacene are promising candidates since they represent organic high charge carrier mobility materials and they are compatible with high-density patterning techniques such as photo-lithography [9,10].

Here, we present organic pin-diodes comprising molecular doped layers of C_{60} and pentacene operating in the ultra-high-frequency region. Three aspects make such pin-diodes favorable in comparison to the Schottky diode approach. Firstly, the current–voltage properties of these elements can be adjusted independently by controlling the thickness of the intrinsic layer or the doping of the charge transport layers. Secondly, the use of doped hole and electron transport layers (HTL/ETL) allows for a free choice of electrode materials and layer sequence which provides an additional advantage concerning integrability. Thirdly, the use of molecular dopants leads to an increased reproducibility which has been demonstrated e.g. for OLEDs [11]. Since we are employing the concept of molecular doping, the influence of dopants on the UHF properties

* Corresponding author.
E-mail address: hans.kleemann@iapp.de (H. Kleemann).

1566-1199/$ - see front matter © 2012 Elsevier B.V. All rights reserved.
http://dx.doi.org/10.1016/j.orgel.2012.03.011

of the pin diodes needs to be considered. On the one hand, molecular doping is a suitable method to control the distance between the electrochemical potential and the charge transport level [12]. Thus, it can help to improve the conductivity. On the other hand, even if dopant states act as shallow acceptors/donors they are impurities which can decrease the conductivity. Therefore, they affect charge carrier transport.

In this publication we present the first UHF organic pin-diodes and we study their electrical small signal and large signal properties. We disclose an optimized doping ratio, where a maximum of conductivity is achieved and where the presence of molecular dopants does not lead to a reduced electrical rectification.

2. Experimental

The devices are prepared on cleaned (supersonic treatment in acetone, ethanol and isopropanol for 5 min and O_2 plasma etching) glass substrates. Metals and organic materials are deposited by thermal evaporation under high-vacuum conditions (base pressure $p < 10^{-7}$ mbar) without breaking the vacuum during sample preparation. The organic layers are sandwiched between a bottom contact (aluminum) and a top contact (aluminum) structured by deposition through shadow masks. Therefore, the active area is defined by the overlap of both contacts. For sake of comparison we realized different device geometries with different active areas of 6.38, 0.04, 0.01, or 0.0025 mm^2. Devices that have an active area of 0.01 mm^2 are manufactured in a special geometry (see Fig. 1) that facilitates a characterization beyond 100 MHz. The other device geometries cannot be studied beyond 100 MHz, which is related to the appearance of resonances caused by wiring. Furthermore, to warrant applicability at UHF conditions we employed a top and bottom metal thickness of 300 nm. This significantly reduces series resistances and improves thermal heat dissipation. The evaporation conditions and sequences of the organic hole transport layer (HTL), the intrinsic interlayer (IIL), and the electron transport layer (ETL) can be taken from the captions of the individual figures. The thicknesses and deposition rates are confirmed by quartz crystal monitoring. Deposition rates are 0.2 nm/s in case of pentacene and 0.05 nm/s in case of C_{60}. For p-type doping of the HTL, we use the p-type dopant 2,2-(perfluoronaphthalene-2,6-diylidene) dimalononitrile (F6-TCNNQ). n-Type doping of the ETL is achieved by co-evaporation of C_{60} and the n-type dopant tetra-kis (1,3,4,6,7,8-hexahydro-2H-pyrimido[1,2-a]pyrimidinato) ditungsten(II) ($W(hpp)_4$), which acts as an effective n-type dopant. Pentacene is purchased from Sensient and C_{60} from Bucky, USA. A Keithley 2400 SMU is used for current–voltage (I–V) characterization. For high-frequency characterization ($\leqslant$20 MHz) of the pin-diodes we used an Agilent 33220A arbitrary waveform generator to apply a sinusoidal voltage. Current and voltage across the diode are monitored by a HP Infinium 500 MHz (bandwidth) 1 GSa/s oscilloscope (input resistance 1 MΩ). For rectification measurements we employed a small circuit containing the diode and a load that consists of a 1 MΩ resistance and a 39 nF capacitor in parallel (see inset Fig. 4(a)). For UHF characterization we utilized a special sample layout

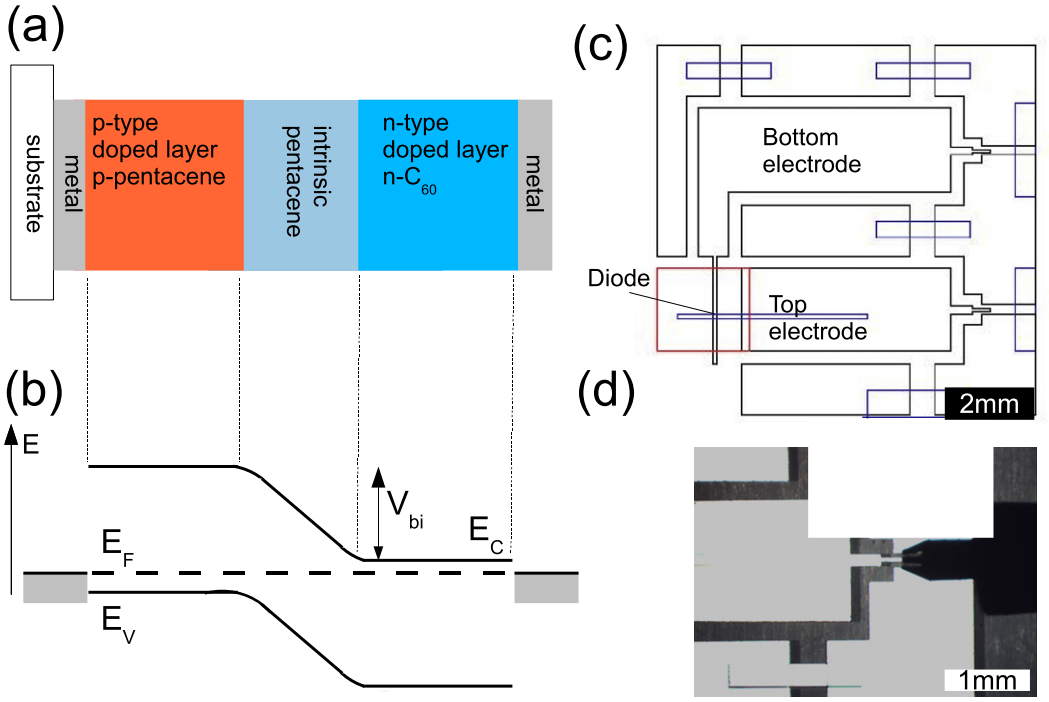

Fig. 1. (a) Layer sequence of an organic pin-diode. (b) Schematic energy level diagram of a pin-diode as drawn in (a). E_C and E_V denote the energy of the conductance and valence state, respectively. E_F denotes the electrochemical potential. (c) Illustration of the used device geometry for UHF characterization. (d) Photograph of diode contact region with microwave probe contacting the device.

fitting to a conventional wafer prober stage. Moreover, also another signal generator (Agilent E8257D) and another oscilloscope (Agilent MSO 6034A, 300 MHz) have been used. For small signal analysis we employed a Rhode& Schwarz ZVL 6 network analyzer.

3. Results and discussion

In order to accomplish operation of organic diodes in the UHF region, several requirements for the electric behavior need to be fulfilled. The diodes have to show small forward resistances, large reverse resistances (large rectification ratios), and small capacitances. The optimization of these parameters are discussed in the first part of this contribution. In the second part we examine the response of these diodes to UHF sinusoidal signals.

The main parameter to adjust the rectification ratio and the capacitance is the interlayer thickness. Firstly, the interlayer thickness determines the current in backward direction as the voltage drops mainly across this layer. Secondly, the reverse capacitance is also dominated by the intrinsic interlayer thickness, as the charge depletion zones at the interface between doped layer and intrinsic layer are typically thinner than the intrinsic layer itself [13]. Thus, thick interlayers are indispensable in order to achieve large rectification ratios and small reverse capacitances.

However, due to the low charge carrier mobility in organic materials the transit time increases for thicker interlayers. Therefore, an optimum of intrinsic interlayer thickness has to be found in order to achieve large rectification ratios as well as a minimum of transit time.

The DC current–voltage curves of pin- and nip-structures are presented in Fig. 2. For discussion of these curves we adopt Shockley's theory for non-ideal diodes [14]. We can differentiate three regions in the *I–V* curves. For small forward (<0.3 V) voltages and the entire reverse direction shown here, the *I–V* curves are dominated by leakage currents (Region I). For forward voltages between 0.3 V and approximately 0.6 V, we obtain an exponential rise of the *I–V* curve (Region II). In this region charge carriers are injected into the intrinsic layer, they diffuse to the other transport layer and recombine. Finally, for forward voltages >0.6 V we observe a space charge limited (SCLC) behavior [16] (Region III), which is superimposed by the exponential current rise of the diode. Charge carrier mobility can be evaluated by SCLC laws to be $\sim 0.2\ \mathrm{cm}^2/(\mathrm{V\,s})$ within the intrinsic layer. However, it should be noticed that we do not obtain a pure SCLC regime (thickness dependency fulfilled, but $\log I \sim V^n,\ n = 2.1$) and accordingly the value for charge carrier mobility is an estimation. The charge carrier mobility is presumably underestimated owing to the presence of charge carrier traps and the effect that the applied voltage is reduced by the built-in potential of the diode.

The *I–V* curves of pin and nip are nearly equal in Regions II and III. This demonstrates that such UHF diodes can be fabricated independently of the layer sequence (pin or nip) which exhibits a remarkable advantage concerning device integration in double- or full-wave rectifier circuits.

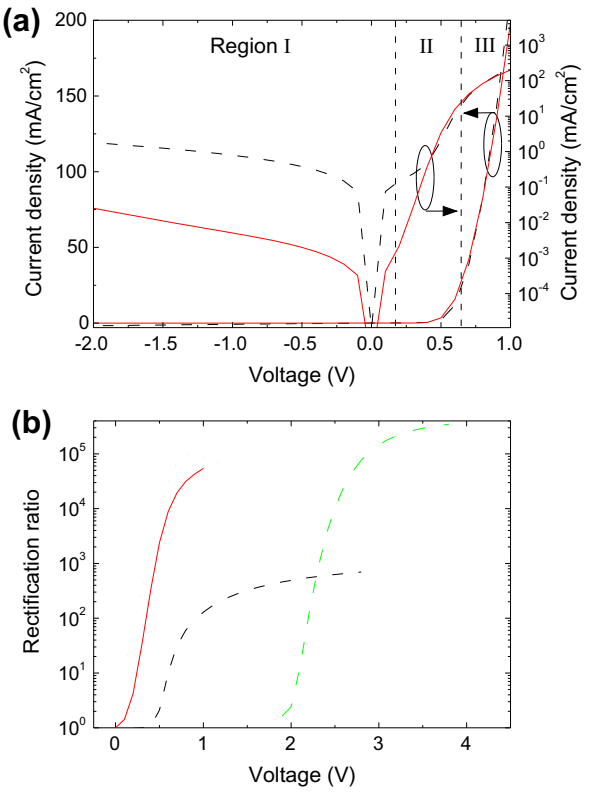

Fig. 2. Current–voltage curves for pin- (red line) and nip-diodes (black dashed line). The layer sequence is Al (50 nm)/pentacene:F6-TCNNQ (50 nm, 1 wt.%)/pentacene (150 nm)/C_{60}:W(hpp)$_4$ (50 nm, 4 wt.%)/Al (100 nm) in case of pin and Al (50 nm)/C_{60}:W(hpp)$_4$ (50 nm, 8 wt.%)/pentacene (110 nm)/pentacene:F6-TCNNQ (50 nm, 4 wt.%)/Al (100 nm) in case of nip. (b) The rectification ratio for a pin (red line), a nip (black dashed line), a typical silicon diode (dashed doted blue), and a wide gap organic diode (light green) as reported elsewhere [15]. (For interpretation of the references to color in this figure legend, the reader is referred to the web version of this article.)

Nevertheless, these devices show a significant difference at reverse and low forward voltages, which is caused by a difference in layer morphology and interface formation. Thus, we believe that for pin-diodes the C_{60} molecules are coated conformal along the peaks and valleys of the rough pentacene layer so that a better interface is created between undoped and doped regions.

In Fig. 3, the influence of different interlayer thicknesses (Fig. 3(a)) and different HTL doping concentrations (Fig. 3(b)) on the device performance is shown. For further discussion we focus on pin-diodes. All dependencies presented for pin diodes can be observed for nip-structures as well. As shown in Fig. 3(a), the current density is reduced for increasing interlayer thickness. In forward direction (upper branch) this is due to the series resistance of the interlayer for small voltages and due to the characteristics of the SCLC for larger voltages. In reverse direction we observe almost no difference for different interlayer thicknesses at small voltages indicating a good blocking of reverse charge carrier transport. Nevertheless, with increasing reverse voltage we measure larger currents for thinner interlayers, which can stem from an increased

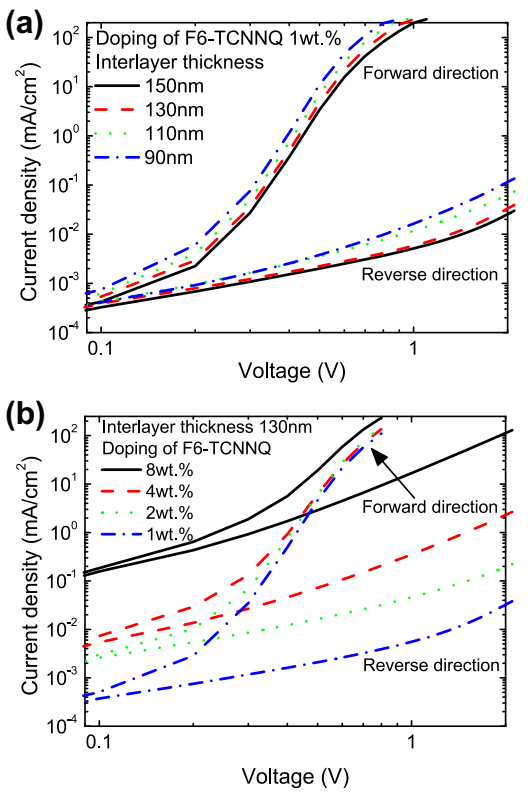

Fig. 3. Current–voltage curves of pin-diodes for different interlayer thicknesses of pentacene (a) and different p-type doping concentrations (b). The layer sequence is Al (50 nm)/pentacene:F6-TCNNQ (50 nm, *x* wt.%)/pentacene (*y* nm)/C_{60}:W(hpp)$_4$ (50 nm, 4 wt.%)/Al (100 nm).

leakage or a field-driven reverse tunneling process [15]. In reverse direction we obtain a reversible junction breakdown at a voltage of −10 V for a interlayer thickness of 90 nm which shifts to more than −20 V for a 150 nm thick intrinsic layer of pentacene. In forward direction a heat induced irreversible breakdown can be observed if the static current density is >50–100 A/cm^2 which appears typically in the range of 4–5 V. However, this thermal damage is not detectable for AC-measurements where we could apply a maximum voltage amplitude of 10 V (signal generator limit). Thus, we conclude that on the one hand one can effectively suppress the reverse current by increasing the interlayer thickness, while on the other hand an increased interlayer thickness leads a reduced forward current and therefore a reduced rectification ratio in total. We obtain an optimum of rectification (9×10^4) for an interlayer thickness of 130 nm of pentacene.

The influence of the doping concentration on forward resistance and leakage current is shown in Fig. 3(b). In reverse direction we observe a clearly reduced leakage current with decreasing doping concentration. This is presumably related to a different morphology of the p-type doped pentacene layer [16] leading to direct shunt paths through the intrinsic interlayer. Apart from this increase in leakage current level, the forward direction is weakly affected for voltages >0.8 V. However, as we reported elsewhere [16], for higher forward voltages where the *I–V* curves are approaching the typical power-law for SCLCs, a reduced mobility with increasing doping concentration is expected. This can be attributed to a reduced crystallinity of doped pentacene. For pin-diodes however, the SCLC regime is dominated by the undoped intrinsic interlayer and therefore if the loss in mobility in the doped layers is moderate the total space charge current is only weakly affected. Thus, for moderate doping where the conductivity of pentacene is strongly increased [16] while charge carrier mobility is almost maintained, controlled doping of pentacene is a key technology to adjust the performance of these pin-diodes. In particular, the reduced leakage level for low doping concentrations causes an increased rectification ratio with an optimum at a doping ratio of 1 wt.% F6-TCNNQ. For doping concentrations less than 1 wt.%, we obtain an additional voltage drop over the HTL, which causes reduced forward currents.

The doping concentration and the interlayer thickness are the key parameters that are technically adjustable in order to optimize the *I–V* performance of such diodes. Thus, we discuss how one can use this knowledge for organic UHF pin-diodes with optimized output characteristics. The active device area is reduced in order to overcome restrictions by the geometrical capacitance of the diode. In Fig. 4(a) we show the DC output voltage of a rectification circuit (see inset) for a sinusoidal input signal (amplitude 2 V) varying the frequency from 1 kHz to 20 MHz. This DC output voltage is displayed for devices having an active area of 0.0025, 0.01, and 0.04 mm^2, respectively. The rectification circuit provides a nearly constant DC voltage over a broad frequency range. However, we observe a drop in DC voltage output for frequencies >10 MHz indicating a limitation by the internal RC time (series resistance of the organic layers times geometrical capacitance) of the diode. This time constant, however, is independent of the area since vertical devices are considered here. Nevertheless, low capacitance devices are favorable since the series resistance which is related to wiring does not scale in the same manner if the device area is reduced. If the DC output voltage is compared for different active areas, one can observe a reduced DC output for smaller active areas. This behavior originates from a changing ratio between the external load and the series resistance of the diode. Thus, if the active area is reduced the series resistance of the diode is enlarged in comparison to the load circuit leading to a reduced DC output.

In Fig. 4(b) we present time resolved measurements of the rectified sinusoidal input signal (20 MHz, amplitude 2 V). For 0.04 mm^2 we do not obtain a strong loss in output performance going from low frequencies to 20 MHz and thus we reach a DC output voltage of almost 1.4 V for a sinusoidal input signal of 2 V amplitude at 20 MHz.

As also shown in Fig. 4(b), we obtain a dependency of the output voltage on the doping concentration. The highest output voltage for 0.0025 mm^2 devices is achieved for a doping ratio of 1 wt.% of F6-TCNNQ in pentacene. As mentioned before, we observe ohmic losses across the HTL for lower doping ratios. For doping ratios >1 wt.% of F6-TCNNQ, we also observe a reduced voltage output even if larger current densities can be observed in the forward *I–V* characteristics (see Fig. 3(b)). This additional loss in

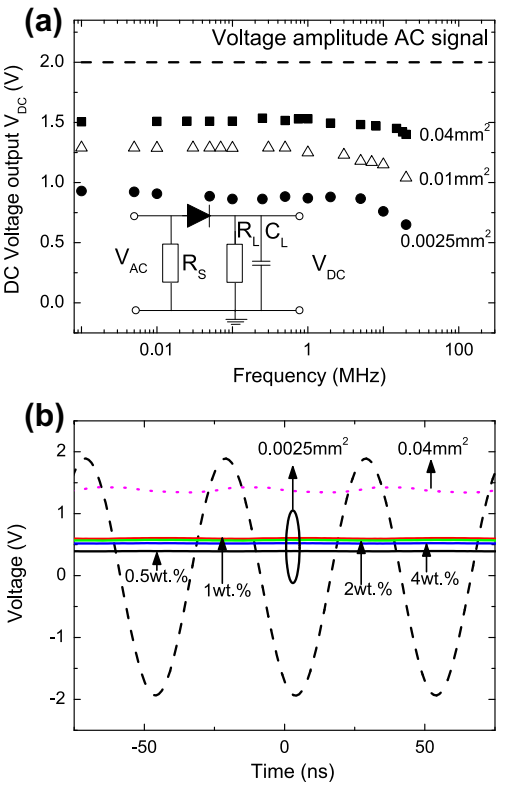

Fig. 4. (a) Frequency dependence of the DC output voltage of organic pin-diodes for a sinusoidal input voltage (dashed line) of 2 V amplitude measured in a rectifier circuit (see inset). Closed boxes represent a pin-diode with an area of 0.04 mm^2 (interlayer thickness 90 nm), open triangles 0.01 mm^2 (interlayer thickness 120 nm), and closed circles 0.0025 mm^2 (interlayer thickness 110 nm). The inset displays the employed rectifier circuit with $R_S = 50\ \Omega$, $R_L = 1\ M\Omega$, and $C_L = 39$ nF. (b) Time resolved response of an organic pin-diode to a sinusoidal input voltage (dashed line) of 20 MHz and an amplitude of 2 V. The colored lines show the output voltage for different p-type doping concentrations measured over a 1 MΩ/39 nF load for 0.04 mm^2 and 0.0025 mm^2 devices. The layer sequence for the pin-diodes is Al (300 nm)/pentacene:F6-TCNNQ (50 nm, *x* wt.%)/pentacene (200 nm)/C_{60}:W(hpp)$_4$ (50 nm, 1–2 wt.%)/Al (300 nm) and the colored lines denote 0.5 wt.% (black), 1 wt.% (red), 2 wt.% (green), and 4 wt.% (blue) of F6-TCNNQ in pentacene. The dotted and magenta colored line (same device as closed boxes in (a)) represents a pin-diode on 0.04 mm^2 with the same layer sequence as the 0.0025 mm^2 devices for a p-type doping concentration of 1 wt.% of F6-TCNNQ. (For interpretation of the references to color in this figure legend, the reader is referred to the web version of this article.)

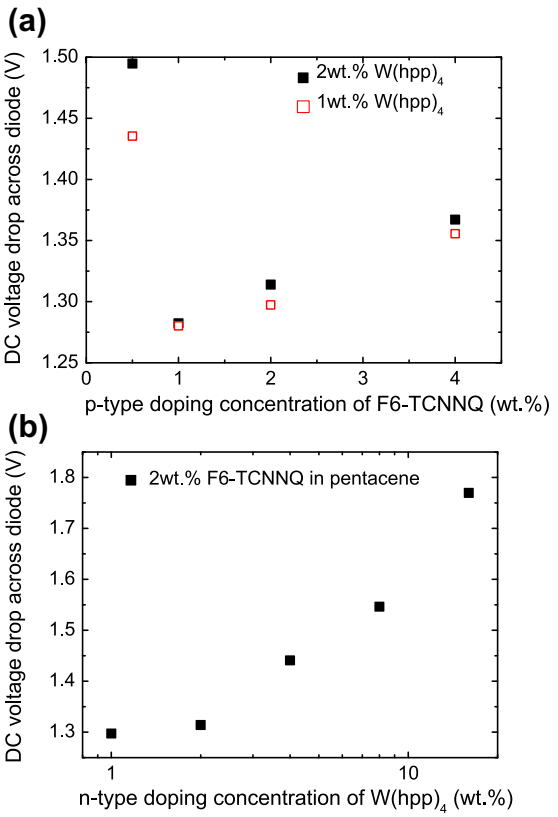

Fig. 5. Voltage drop over the diode (input voltage amplitude minus the voltage measured over the load) for different p-type (a) and n-type (b) doping concentrations (input voltage 20 MHz, 2 V amplitude, active area 0.0025 mm^2). The layer sequence for devices shown in (a) and (b) is described in the caption of Fig. 4. The last two points (8 wt.% and 16 wt.% of W(hpp)$_4$ in C_{60}) in (b) are recorded for nip structures as described in the caption of Fig. 2 with an interlayer thickness of 110 nm.

output voltage is likely caused by the increased leakage level and subsequently the reduced rectification ratio. Accordingly, the reduced rectification ratio gives rise to a discharging of the load capacitor via the reverse resistance of the diode in addition to the load resistance. The loss in DC output voltage for different p- as well as n-type doping concentrations is shown in Fig. 5. In particular, for p-type doping we find an optimum in DC output voltage for 1 wt.% F6-TCNNQ in pentacene, where we have the smallest leakage current but still an effective doping reducing contact and layer resistance. For n-type doping we do not reach such an optimum. However, from the saturation behavior between 1 wt.% and 2 wt.% of W(hpp)$_4$ in C_{60} (see Fig. 5(b)) we conclude that 1 wt.% of doping is close to that optimum. Devices with a doping concentration of 0.5 wt.% of W(hpp)$_4$ in C_{60} are not working stable. This is likely caused by the appearance of an interface barrier between the doped C_{60} layer and the metal contact. Fig. 5 clearly shows that we can gain more than 0.5 V in output voltage for devices with optimized doping ratios. It should be mentioned that the absolute value of the voltage drop across the diode depends on the device geometry as well as the external load. Therefore, it is merely used to compare the output characteristics of equivalent devices having the same geometry and being connected to the same external circuit.

The main argument for the optimized performance at 1 wt.% F6-TCNNQ doping concentration is the reduced leakage current. However, from a physical point of view the dynamics of charge carrier transport in the doped layers are of particular interest. Are dopants acting as scattering centers or do they even destroy the molecular arrangement? For both materials doping can cause a loss in mobility. While for C_{60} a continuous decay in mobility by doping is reported [17], an abrupt transition is observed for pentacene [16]. This transition in mobility is caused by a structural phase transition in pentacene induced by the molecular dopants. In case of F6-TCNNQ this structural

phase transition appears for a doping concentration of approximately 4 wt.%. As discussed, the pin-diodes obey in forward voltage direction a SCLC law which is governed by the intrinsic interlayer. Subsequently, a moderate loss in charge carrier mobility within the doped charge transport layers does not necessarily lead to a reduced forward current. This is related to the fact that the doped charge carrier transport layers are significantly thinner than the intrinsic layer. Therefore, for the considered range of doping the loss of mobility is not dominating the diode performance and thus also not the cut-off frequency. For larger dopant concentrations such effects might appear. However, they are likely superimposed by other effects induced upon doping such as the increased leakage current level.

The role of the interlayer thickness at ultra-high frequencies is twofold. First, it determines the characteristic RC product of the layer resistance R and its capacitance C and second, it determines the ratio between the external load and the impedance of the diode. In Fig. 6 we show the influence of the interlayer thickness on the DC output voltage at 20 MHz. In accordance to the previous discussion, a reduced interlayer thickness leads to a reduced series resistance of the diode and therefore to a smaller voltage loss across the diode. Thus, the linear behavior between voltage loss and interlayer thickness can be understood by a voltage divider between the load resistance and the series resistance of the diode. In other words: the thinner the interlayer, the larger the DC voltage output. Unfortunately, in the present case a minimum of interlayer thickness is required in order to provide a sufficient blocking of reverse current. A thickness of 90 nm pentacene exhibits an optimum for the trade-off between lowest forward resistance and highest reverse resistance.

To highlight the potential of the presented diodes at UHF conditions, we designed a special layout (see Fig. 1(c) and (d)) in order to warrant resonance free electric conduction of the incoming UHF field. This has been proven by a small signal analysis of the employed structure. As shown in the inset of Fig. 7 we obtain a negative phase which indicates a dominating capacitive behavior which originates from the geometrical capacitance of the diode (~4–5 pF). Between 1 MHz and 1 GHz the device behaves like an ideal RC-unit which can be seen in the decrease of the magnitude of the impedance $|Z|$ ($|Z| \sim 1/f$). For increasing frequency f the phase is increasing and a first resonance due to the inductance of electrical leads and the diode capacitance occurs at 1 GHz. This allows for a quantitative analysis of the rectifier circuit below 1 GHz. Thus, in the setup as shown in Fig. 1(d), the diodes have been characterized up to a frequency of 300 MHz which is the limit of our oscilloscope. As shown in Fig. 7, we obtain an almost constant DC output voltage in the range from 1 kHz to 10 MHz. Beyond 10 MHz the rectified DC voltage drops with increasing frequency. Nevertheless, at 300 MHz we still obtain a DC voltage of 0.5 V with a small ripple amplitude of 0.13 V. From this we can estimate that these diodes are able to provide a DC output voltage up to frequencies close to 1 GHz.

This estimation is in accordance to transit time predictions. Two different approaches have been suggested in this context. In a first transit time model the maximum frequency f_{max} is derived according to [1]

$$f_{max} = \frac{1}{\tau} = \frac{\mu}{L^2}(V_A - V_{DC}), \quad (1)$$

where τ is the transit time, μ the mobility, L the length of the device, V_A the amplitude of the applied AC signal and V_{DC} the DC voltage measured across the load resistance. However, this simple model assumes a constant field in the diode and does not take into account the field dependent mobility of organic materials. Therefore, the maximum frequency is underestimated by this model. The second approach, reported by Steudel et al. [1,5], derives the maximum frequency as

$$f_{max} = \frac{9\mu}{16\pi L^2 V_{DC}}\left((V_A^2 + V_{DC}^2)arccos\left(\frac{V_{DC}+V_F}{V_A}\right) + \left(-3V_{DC}+V_F\right)\sqrt{V_A^2-(V_{DC}+V_F)^2}\right), \quad (2)$$

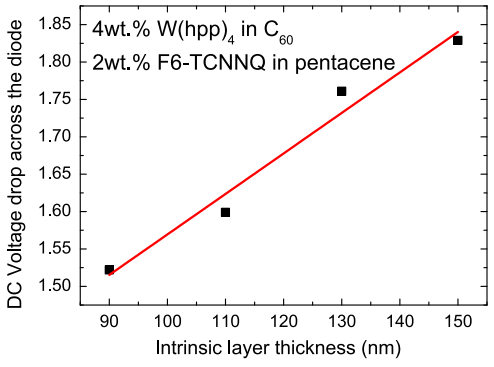

Fig. 6. Voltage drop over the diode for different interlayer thicknesses (input voltage 20 MHz, 2 V amplitude, active area 0.0025 mm^2) in case of a pin-diode. The layer sequence is as described in the caption of Fig. 3. The red line shows a linear fit of the data points. (For interpretation of the references to color in this figure legend, the reader is referred to the web version of this article.)

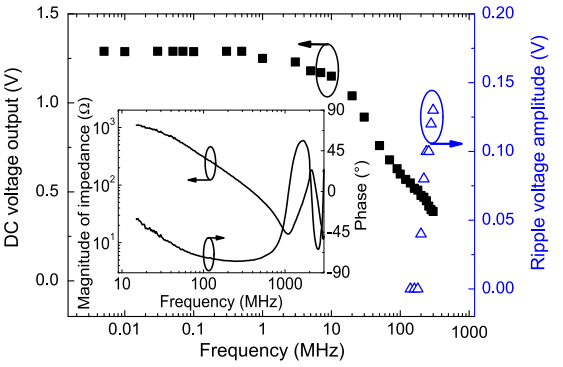

Fig. 7. Frequency dependence of the DC output voltage and the ripple voltage amplitude of an organic pin-diode for a sinusoidal input voltage of 2 V amplitude. The active area of the pin-diode is 0.01 mm^2 and the device layout is sketched in Fig. 1(c). The layer sequence for the pin-diodes is Al (300 nm)/pentacene:F6-TCNNQ (50 nm, 2 wt.%)/pentacene (120 nm)/C_{60}:W(hpp)$_4$ (50 nm, 1 wt.%)/Al (300 nm). The inset displays the results of the small signal analysis of the rectifier structure with shortcut instead of an external load.

where V_F is the transition voltage (where the SCLC regime starts) of the diode, assuming space charge limited currents. Thus, it is mainly suited for voltages larger than V_F, where the diode shows clear SCLC behavior. Accordingly, both approaches cannot provide exact values for the maximum frequency in case of the low voltage pin-junctions reported here. Nevertheless, we utilized Eq. (1) to estimated a limit for the cut-off frequency. Relying upon a charge carrier mobility of $\sim$0.2 cm^2/(V s), taking an intrinsic layer thickness of 120 nm, and a DC voltage of 1.25 V, one can compute a cut-off frequency of $\sim$1.04 GHz which is in accordance to our experimental finding. However, this is a lower limit for cut-off frequency since Eq. (1) is derived under the assumption of an Ohmic behavior. Thus, the stronger voltage dependence of the SCLC will lead to a higher cut-off frequency.

It is the intention of current experiments to shift this limit to higher frequencies by further optimization of layer thickness, doping concentration, and device layout. In particular, the interlayer thickness of pentacene is a crucial parameter that governs the frequency limit. We presume that by varying deposition conditions for pentacene the required layer thickness can be further reduced leading to a higher cut-off frequency. Furthermore, to get a deeper insight into the underlying microscopic processes, we will focus in future experiments on the relation between important small signal quantities of the diodes such as charge carrier lifetime and charge-transfer time [18] and the large signal cut-off frequency.

4. Conclusion

We present organic pin- and nip-diodes with an adjustable current voltage performance operating at UHF conditions. The influence of different doping concentrations and different intrinsic interlayer thicknesses on the DC device performance is studied. In particular, we show that for the chosen structure comprising C_{60} and pentacene the overall leakage current level increases with increasing doping concentration. While the forward voltage performance of these diodes cannot be improved for larger doping concentrations, the effect of increased leakage leads to a reduced rectification ratio with increasing doping concentration. Moreover, we point out that for the presented device structure a thickness of the intrinsic interlayer of 130 nm provides the largest rectification ratio 10^5. By this knowledge we are able to present organic diodes with an optimized I–V performance working at frequencies up to 300 MHz. Furthermore, we can demonstrate an improvement in DC output voltage by 0.5 V for an optimized doping concentration and a proper intrinsic layer thickness. For optimized devices we obtain a DC voltage output of almost 1.4 V for a sinusoidal input signal of 20 MHz and an amplitude of 2 V. From UHF measurements up to 300 MHz we can estimate a cut-off frequency of these diodes in the range of 1 GHz.

Acknowledgments

The authors thank Novaled AG and the state of Saxony for financial support in project NKOE (12712) and Novaled AG for providing dopant materials. The work leading to these results has received funding from the European Community's Seventh Framework Programme under Grant Agreement No. FP7-267995 (NUDEV).

References

[1] S. Steudel, K. Myny, V. Arkhipov, C. Deibel, S. de Vusser, J. Genoe, P. Heremans, Nat. Mater. 4 (2004) 597.
[2] L. Ma, J. Ouyang, Y. Yang, Appl. Phys. Lett. 84 (2004) 4786.
[3] B. Pal, J. Sun, B. Jung, E. Choi, A. Andreou, H. Katz, Adv. Mater. 20 (2008) 1023.
[4] K. Myny, S. Steudel, P. Vicca, J. Genoe, P. Heremans, Appl. Phys. 93 (2008) 093305.
[5] S. Steudel, K. Myny, P. Vicca, D. Cheyns, J. Genoe, P. Heremans, in: IEEE International Electron Devices Meeting, vol. 4, 2008.
[6] K. Myny, S. Steudel, P. Vicca, M. Beenhakkers, N. van Aerle, G. Gelinck, J. Genoe, W. Dehaene, P. Heremans, Solid State Electron. 53 (2009) 1220.
[7] C. Kang, S. Kim, Y. Hong, C. Lee, Thin Solid Films 518 (2009) 889.
[8] D. Im, H. Moon, M. Shin, J. Kim, S. Yoo, Adv. Mater. 23 (2011) 644–648.
[9] P. Taylor, J.-K. Lee, A. Zakhidov, M. Chatzichristidi, H. Fong, J. DeFranco, G. Malliaras, C. Ober, Adv. Mater. 21 (2009) 2314–2317.
[10] H. Kleemann, A. Zakhidov, T. Menke, M. Anderson, K. Leo, B. Lussem, Org. Electron. 13 (2012) 506.
[11] R. Meerheim, B. Lussem, K. Leo, Proc. IEEE 97 (2009) 1606.
[12] S. Olthof, W. Tress, R. Meerheim, B. Lussem, K. Leo, J. Appl. Phys. 106 (2009) 103711.
[13] H. Kleemann, B. Lussem, K. Leo, J. Appl. Phys., submitted for publication.
[14] K. Harada, A. Werner, M. Pfeiffer, C. Bloom, C.M. Elliott, K. Leo, Phys. Rev. Lett. 94 (2005) 033601.
[15] H. Kleemann, R. Gutierrez, F. Lindner, S. Avdoshenko, P. Manrique, B. Lussem, G. Cuniberti, K. Leo, Nano Lett. 10 (2010) 4929.
[16] H. Kleemann, C. Schunemann, A. Zakhidov, B. Lussem, K. Leo, Org. Electron. 13 (2012) 58.
[17] K. Harada, F. Li, B. Maennig, M. Pfeiffer, K. Leo, Appl. Phys. Lett. 91 (2007) 092118.
[18] P. Peumans, V. Bulovic, S. Forrest, Appl. Phys. Lett. 76 (2000) 3855.